Annals of Nuclear Energy 63 (2014) 51–58

Contents lists available at ScienceDirect

Annals of Nuclear Energy

journal homepage: www.elsevier.com/locate/anucene

Numerical simulation of convection of argon gas in fast breeder reactor

Dinesh Nath [a], Mahendra K. Verma [b,*]

[a] Nuclear Engineering and Technology Program, Indian Institute of Technology, Kanpur 208016, India
[b] Department of Physics, Indian Institute of Technology, Kanpur, UP 208016, India

ARTICLE INFO

Article history:
Received 1 September 2012
Received in revised form 15 July 2013
Accepted 16 July 2013

Keywords:
Annulus convection
Turbulent convection
Fast breeder reactor

ABSTRACT

In this paper, we present the results of numerical simulations of the turbulent convection in the Argon gas present in the annulus of a fast breeder reactor. We employ RANS scheme with k–ϵ model and solve the equations using an open-source software OpenFOAM. The Rayleigh numbers Ra of our simulations lie in the range of 10^8 to 10^{10}. We observe a pair of rolls with a hot plume rising from one end, and a cold plume descending from the opposite end of the annulus. This feature results because the aspect ratio of the geometry is near unity. We also find that the circumferential temperature difference (CTD) is proportional to Ra.

1. Introduction

In a pool type fast breeder reactors (FBR), schematically represented in Fig. 1, many mechanical components such as pumps, intermediate heat exchanger (IHX), rotating plugs, and control plugs are penetrated from the roof of the reactor vessel (Velusamy et al., 2010). These penetrations create vertical annulus which are closed at the top and open inside the reactor vessel. Argon gas, used as a cover gas over the liquid sodium in the reactor vessel, occupies the annular spaces as shown in Figs. 1 and 2. The liquid sodium is at a temperature of approximately 800 K, and it must be strictly separated from the open air. The sidewall of the cylindrical annulus and the top enclosure at the roof are cooled by an external circuit of air to maintain its temperature at around 400 K (Fig. 2). Convective rolls are created due to the temperature difference between the roof-top and bottom opening. The hot and light gas above the liquid sodium enters the annulus, loses heat to the annulus walls thus becoming heavier, and comes down the annulus at another circumferential location. This phenomenon of natural convection in the annulus results in a non-uniform circumferential temperature distribution in the penetrating component. This uneven temperature distribution causes uneven expansion near the walls of the annulus thus creating stresses which could cause deflection or tilting of components. These deformations would be detrimental to the operation of the reactor. A safe usage of reactors requires the deflections to be within a certain limit, hence, a good knowledge of the circumferential temperature distribution in the annulus is essential. In this paper, we perform numerical simulations of natural convection of Argon in the Fast Breeder reactor, and study the circumferential temperature distribution in the annulus as a function of system parameters. Several experiments related to the turbulent convection in PFBR annulus have been performed. Vijayan et al. (1986) performed experiments in a vertical annulus with water as the working fluid, and studied the variation of the temperature profile and Nusselt number as a function of Rayleigh numbers (Ra). They also studied the effects of baffles on the flow. The exponent of the Nusselt number varied from 0.342 in the absence of baffles to 0.182 with baffles. Hemanath et al. (2007) and Meikandamurthi et al. (1991) performed experiments in a vessel similar to PFBR and studied the flow properties of Ar gas, which was heated by the liquid sodium from below. They observed a logarithmic increase in the CTD with the increase of Ra from 10^8 to 10^{10}. Hemanath et al. (2007) have further shown that cooling the sidewalls markedly reduce CTD, but the use of helium gas instead of Ar does not affect the CTD significantly. Yamakawa and Sakai (1986) arrived at similar conclusions in an experiment on IHX with water as a fluid. Earlier Timo (1954) had studied the heat transfer in an annulus using experiments and theoretical modeling. In all the above experiments, the researchers typically observed a pair of convective rolls.

A large number of numerical simulations have been performed to understand the flow profile in the annulus of PFBR. Yamakawa and Sakai (1986) performed numerical simulations using a three-dimensional computational fluid dynamics code THERVIS III and found consistency with experiments. They observed that the flow patterns inside the annulus depends quite critically on the radiative heat loss from the sidewalls. Hemanath et al. (2007) simulated the system using the PHEONICS code and observed behavior simi-

* Corresponding author. Tel.: +91 512 2597396; fax: +91 512 2590914.
E-mail address: mkv@iitk.ac.in (M.K. Verma).
URL: http://home.iitk.ac.in/~mkv (M.K. Verma).

0306-4549/$ - see front matter © 2013 Elsevier Ltd. All rights reserved.
http://dx.doi.org/10.1016/j.anucene.2013.07.021

Nomenclature

$\bar{x}$	resolved position (m)	ε	turbulent dissipation rate ($m^2\ s^{-3}$)
$\bar{u}$	resolved velocity ($m\ s^{-1}$)	l	turbulent length scale (m)
$\bar{p}$	resolved pressure ($kg\ m^{-1}\ s^{-2}$)	D	diameter of the annulus (m)
T	resolved temperature (K)	δ	annulus gap (m)
T_0	reference temperature (K)	L	length of annulus (m)
U	mean velocity ($m\ s^{-1}$)	H	height of the whole geometry (m)
P	mean pressure ($kg\ m^{-1}\ s^{-2}$)	ΔT	axial temperature difference
ρ	density ($kg\ m^{-3}$)	Q	heat flux (J)
β	thermal expansion coefficient (K^{-1})	Pr	Prandtl Number
ν_0	viscosity ($m^2\ s^{-1}$)	Pr_t	turbulent Prandtl Number
ν_t	turbulent viscosity ($m^2\ s^{-1}$)	Ra	Rayleigh Number
α	thermal diffusivity ($m^2\ s^{-1}\ K$)	ϵ_1	$= \frac{L}{\pi D},\ \epsilon_2 = \frac{L}{\delta}$
α_t	turbulent diffusivity ($m^2\ s^{-1}\ K$)	Λ_1	$= 1/\epsilon_1,\ \Lambda_2 = 1/\epsilon_2$: aspect ratios
g	gravity ($m\ s^{-2}$)	Ra	$= \frac{g\beta\Delta T L^3}{\nu^2}\mathrm{Pr}$
k	turbulent kinetic energy ($m^2\ s^{-2}$)		

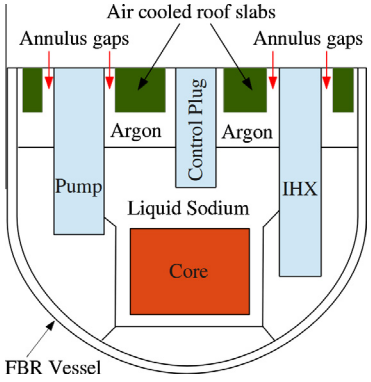

Fig. 1. A schematic view of the prototype fast breeder reactor (PFBR).

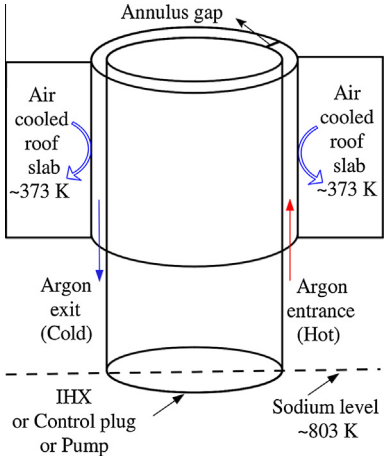

Fig. 2. A zoomed view of the annulus of a PFBR. The air gap between the wall and the component is around 5–10 mm.

lar to their experiments. Velusamy et al. (1998) applied computer codes THYC-2D and COND-2D to simulate the flow and studied the effects of air inlet temperature and gap width on the turbulent flow. In a recent numerical work Paliwal et al. (2012) studied the flow pattern for much larger gap-width (50 mm) and diameters, and observed very different results. For example, they obtain two to ten convective cells for different aspect ratios. Baldassari et al. (1984) and Goldstein and Joly (1979) have also simulated the flow in the annulus and observed results similar to those described above.

Numerical simulation of convective turbulence is very challenging since it involves a wide range of length and time scales. We require very high resolution direct numerical simulations (DNS) with small time steps to resolve the large range of length- and time scales. These direct simulations require large supercomputers, hence they are not always practical for many complex engineering problems. An alternate approach is to perform simulations on a coarser grid with an appropriate modeling of the small-scale turbulence. Two major methods in this class are the Reynolds-averaged Navier Stokes (RANS) and the Large Eddy Simulations (LES). In the RANS approach, we time average the Navier–Stokes equation which produces an additional term, generally referred to as Reynolds stress. This term is simplified using appropriate turbulence models. In the LES schemes, an spatial filtering is performed, and enhanced diffusive parameters are employed to take care of the turbulence at smaller scales. In the present paper we employ a RANS scheme for studying the turbulent convection in PFBR, with the Reynolds stress modeled using the k–ϵ model.

In this paper we simulate the convective turbulence in the annulus of PFBR using OpenFOAM (Open Source Field Operation and Manipulation). Using these simulations we study the circumferential temperature difference (CTD), and the velocity and temperature profiles for two different geometries, including the geometry used in the COBA test facility at the Indira Gandhi Centre for Atomic Research (IGCAR), Kalpakkam, India. The largest Rayleigh number used for our simulation is 1.52×10^{10}. The numerical method and equations are discussed in Section 2, while the numerical results are described in Section 3. We conclude in Section 4.

2. Numerical method and geometrical configuration

As discussed in the introduction, a direct numerical simulation of convective flows for large Rayleigh numbers require extremely fine grid and a large amount of computer time. Therefore we resort to RANS type simulation with a coarser grid, and the Reynolds stress prescribed using k–ϵ model. We solve the following RANS-averaged incompressible fluid equations:

$$\frac{\partial \overline{u_j}}{\partial x_j} = 0, \tag{1}$$

$$\frac{\partial \overline{u_i}}{\partial t}+\frac{\partial}{\partial x_j}(\overline{u_j u_i})-\frac{\partial}{\partial x_j}\left\{\nu_{eff}\left[\frac{\partial \overline{u_i}}{\partial x_j}+\frac{\partial \overline{u_j}}{\partial x_i}\right]\right\}=-\frac{\partial \overline{p}}{\partial x_j}+g[1-\beta(\overline{T}-T_0)], \tag{2}$$

$$\frac{\partial \overline{T}}{\partial t}+\frac{\partial}{\partial x_j}(\overline{T u_j})=\left(\frac{\nu_0}{\mathrm{Pr}}+\frac{\nu_t}{\mathrm{Pr}_t}\right)\frac{\partial^2 \overline{T}}{\partial x_k^2}. \tag{3}$$

We assume incompressibility, which is a good assumption since the flow speeds are much smaller than the sound speed. The variation in the density ρ is approximated according to the Boussinesq approximation as $\rho=\rho_0(1-\beta(\overline{T}-T_0))$, where ρ_0 is a density of Argon corresponding to the temperature T_F, which is the temperature of the floor (see Figs. 3 and 4). According to the k–ϵ model, the turbulent viscosity is modeled as $\nu_t=C_\mu k^2/\epsilon$, where the dissipation rate $\epsilon=C_\mu^{0.75}k^{1.5}/l$ with l as the length scale, and $C_\mu=0.09$ (a constant). We take Pr_t as described in literature and the OpenFOAM manual.

We use PIMPLE (Pressure Implicit Method for Pressure-Linked Equations) scheme to numerically solve the above equations (Eqs. (1)–(3)). PIMPLE is a hybrid algorithm between PISO (Pressure Implicit with Splitting of Operators, Issa (1985)) and SIMPLE (Semi-Implicit Method for Pressure-Linked Equations, (Patankar, 1980)), with the former being applicable to the transient flows, while the later being more suitable for steady flows. We employ Euler method for time-stepping. The gauss-upwind scheme (Patankar, 1980) of finite volume method is used for the discretization of the divergence term. Preconditioned conjugate gradient (PCG) and Preconditioned bi-Conjugate Gradient (PBiCG) methods (Barrett et al., 1994) are used to solve the final linear set of equations iteratively.

We solve the fluid equations for two geometrical configurations:

- *G1* (Fig. 3): Cylindrical volume at the base, and annulus at the top. This geometry is similar to the COBA setup (Hemanath et al., 2007). The geometrical details of the setup is given in Table 1.
- *G2* (Fig. 4): The component from the roof penetrates up to the base. We carry out simulations for three different configurations, G2.1, G2.2, G2.3, whose parameter values are listed in Table 1.

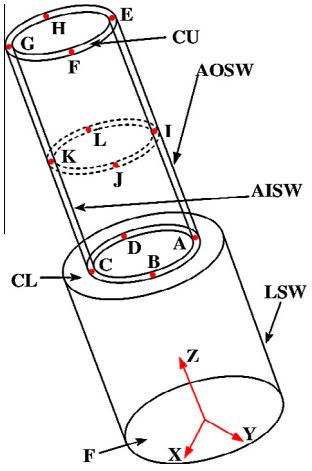

Fig. 3. Geometrical configurations G1 of our simulations. The volume is cylindrical at the base and annulus at the top, similar to the FBR component penetrations. Here F: Floor, CL: Ceiling Lower, CU: Ceiling Upper, AOSW: Annulus Outer Side Wall, AISW: Annulus Inner Side Wall, LSW: Lower Side Wall.

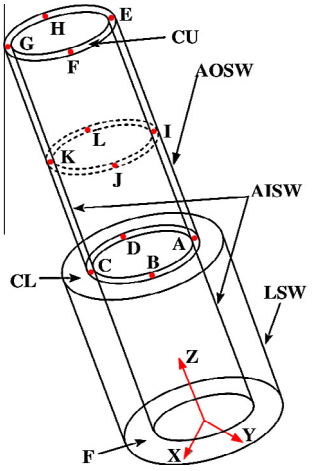

Fig. 4. Geometrical configurations G2 of our simulations. The component penetrates all the way up to the base, thus forming two annuli, one at the top and other at the bottom.

Aspect ratio plays an important role in convective turbulence. If we cut open the annulus, the geometry resembles a cuboid with two aspect ratios $\Lambda_1=2\pi r_{out}/L$ and $\Lambda_2=(r_{out}-r_{in})/L$, where r_{out}, r_{in} are the outer and inner radii of the cylinder respectively. For the geometrical configurations used in our simulations, Λ_1 is of the order of 1, and $\Lambda_2 \ll \Lambda_1$. Hence the flow in the cylinder are expected to be similar to that in a two-dimensional box with the periodic boundary condition along the lateral direction (Paul et al., 2010). Hence we expect to observe a pair of rolls, consistent with the earlier experimental results (Baldassari et al., 1984; Goldstein and Joly, 1979; Hemanath et al., 2007; Lenoir and Goldstein, 1981; Meikandamurthi et al., 1991; Velusamy et al., 1998; Vijayan et al., 1986; Yamakawa and Sakai, 1986) and numerical results (Baldassari et al., 1984; Goldstein and Joly, 1979; Hemanath et al., 2007; Velusamy et al., 1998; Yamakawa and Sakai, 1986). For our simulations, we choose grid resolutions $19\times100\times150$ for G1, G2.1, G.2.2, and $10\times100\times168$ for G2.3, which are comparable to $19\times100\times129$ grid used by Hemanath et al. (2007). The thickness of the annulus is small compared to its radius, so we employ a small number (19) of uniform grid points along the thickness. We have verified our resolution by performing grid independence test on finer grids. We employ a wall function treatment to take care of the boundary layer in our implementation.

We assume a constant temperature for the circulating cool air around the outer-sidewall (AOSW) (shown in Fig. 3). For our simulation we take the temperature of the cooling air to be 373 K. The variable temperature of Argon gas causes dynamic heat flux over the AOSW. Based on Fourier's law and Newton's law of cooling, the following boundary conditions are adopted to model the heat transport from the Argon to the wall (Ar → AOSW), and then from the wall to the air outside (AOSW → air):

Table 1
Geometrical specifications of the annulus: r_{base} is the radius of the floor, $r_{out,in}$ are the outer and inner radii of the annulus respectively, $\delta=r_{out}-r_{in}$, L is the height of the annulus, H is the height of the geometry, $\epsilon_1=L/(2\pi r_{out})$, and $\epsilon_2=L/\delta$.

Geometry	r_{base}	r_{out}	r_{in}	H	L	δ	ϵ_1	ϵ_2
G1	0.233	0.181	0.161	1.8	1	0.02	0.87	50
G2.1	0.233	0.185	0.165	1.8	1	0.02	0.87	50
G2.2	0.233	0.185	0.175	1.8	1	0.01	0.87	100
G2.3	0.233	0.185	0.175	2.6	1.8	0.01	1.54	180

Table 2
Properties of Argon gas used in our simulations (Dwight, 1972). The variables are the thermal expansion coefficients (β), the Prandt number (Pr), the density (ρ), and the thermal diffusivity (α). These parameters are computed using $T_{mean} = (T_F + T_{AOSW})/2$ at $t = 0$.

T_{mean} (K)	588	538	488	438	388
β	2.700	1.858	2.049	2.283	2.577
Pr	0.660	0.662	0.664	0.6678	0.672
ρ	0.909	0.994	1.0963	1.2214	1.378
α	6.280	5.388	4.548	3.762	3.034

$$\left.\frac{\partial T}{\partial n}\right|_{(\mathrm{Ar}\to\mathrm{AOSW})} = \frac{Q|_{(\mathrm{Ar}\to\mathrm{AOSW})}}{\alpha_{\mathrm{eff}}^{\mathrm{Ar}} C_p^{\mathrm{Ar}} \rho^{\mathrm{Ar}}}, \tag{4}$$

$$\left.\frac{\partial T}{\partial n}\right|_{(\mathrm{AOSW}\to\mathrm{air})} = \frac{Q|_{(\mathrm{AOSW}\to\mathrm{air})}}{\alpha_{\mathrm{eff}}^{\mathrm{air}} C_p^{\mathrm{air}} \rho^{\mathrm{air}}}, \tag{5}$$

$$Q|_{(\mathrm{Ar}\to\mathrm{AOSW})} = h_{\mathrm{Ar}}(T_{\mathrm{Ar}} - T_{\mathrm{AOSW}}), \tag{6}$$

$$Q|_{(\mathrm{AOSW}\to\mathrm{air})} = h_{\mathrm{air}}(T_{\mathrm{AOSW}} - T_{\mathrm{air}}), \tag{7}$$

where $\hat{n}$ is the unit normal to the wall. We take heat transfer coefficients of Argon and air to be $h_{\mathrm{Ar}} = 10\ \mathrm{W\,m^{-2}\,K^{-1}}$ and $h_{\mathrm{air}} = 15$ - $\mathrm{W\,m^{-2}\,K^{-1}}$ respectively. We also take the specific heat of air $C_p^{\mathrm{air}} = 1009\ \mathrm{J\,kg^{-1}\,K^{-1}}$, the thermal diffusivity $\alpha_{\mathrm{eff}}^{\mathrm{air}} = 5 \times 10^{-3}\ \mathrm{m^2\,s^{-1}}$, the temperature of cooling air $T_{\mathrm{air}} = 373$ K, the specific heat of Argon $C_p^{\mathrm{Ar}} = 520.34\ \mathrm{J\,kg^{-1}\,K^{-1}}$, and the effective thermal diffusivity of Argon $\alpha_{\mathrm{eff}}^{\mathrm{Ar}} = 2.115 \times 10^{-3}\ \mathrm{m^2\,s^{-1}}$.

We assume Boussinesq approximation under which a single parameter value is used for the viscosity and thermal diffusivity of the fluid. We use the average temperature $T_{mean} = (T_F + T_{AOSW})/2$ (T_F, T_{AOSW} are the temperatures of the Floor and annulus outer side wall (AOSW) respectively) at $t = 0$ to compute these quantities (see Table 2). The temperature difference of the experimental setup is reasonably high (~500degr), consequently v_0 varies from 2.086×10^{-5} (for 373 K) to 6.984×10^{-5} (for 803 K), which is quite significant. However, in the present work we investigate the approximate behavior of the thermal plumes, for which the Boussinesq approximation is a reasonable assumption.

In the next section, we present the numerical results of our simulations.

3. Numerical results

Using OpenFOAM we perform numerical simulations for the two aforementioned geometrical configurations G1 and G2 under the stated boundary conditions. We vary the temperature of the bottom floor from 803 K to 403 K in steps of 100 K. We measure the temperature at different probes shown in Figs. 3 and 4. The temperature probes are A, B, C D at the bottom, E, F, G, H at the top, and I, J, K, L in the middle. The axial temperature difference ΔT is computed by taking the difference between the time-averaged values $(\overline{T_A} + \overline{T_B} + \overline{T_C} + \overline{T_D})/4$ and $(\overline{T_E} + \overline{T_F} + \overline{T_G} + \overline{T_H})/4$ (see Tables 3 and 4). This value of ΔT is used in the computation of Rayleigh number Ra, which ranges from approximately 10^8 to 10^{10}. We apply the boundary conditions listed in Table 5. For the initial condition of all the runs, we take the initial temperature of the fluid as $(T_F + T_{AOSW})/2$, where T_F and T_{AOSW} are the temperatures of the floor and annulus outer side wall respectively. The initial velocity field is taken to be zero.

Table 3
Parameters used in simulations for G1: Floor temperature (T_F), Rayleigh number (Ra), T_{mean} in the annulus, the axial temperature difference ΔT, and circumferential temperature difference (CTD).

T_F (K)	803	703	603	503	403
T_{mean}	547	515	470	430	386
ΔT	51	36	23	12	4
CTD	56	40	19	15	4
Ra	1.64×10^9	1.23×10^9	8.70×10^8	4.90×10^8	1.86×10^8

Using OpenFOAM we study the velocity and temperature profiles of the two geometries G1 and G2. The Rayleigh numbers for these geometries range from 1.86×10^8 to 1.64×10^9, and 1.42×10^8 to 1.52×10^{10} respectively. We observe that the temperature and the velocity fields are highly time-dependent, as evident from the Movies (Movies G12). Sample snapshots of the temperature profiles of G1 and G2 are depicted in Figs. 5 and 6 respectively, with the subfigures (a) exhibiting the temperature variation for the cylinder, while the subfigures (b) exhibiting a verticalcross-section.

3.1. Generic features

We observe certain generic features for both the geometries. These features are listed below.

- In our simulations, typically we observe a swirling pair of rolls (an ascending and descending pair of plumes). However, occasionally the plumes disintegrate into smaller structures. On rare occasions, more than a pair of plumes is observed as well. Refer to videos (Movies G12) for viewing the dynamics. Occurrence of a pair of rolls is due to the fact that the aspect ratio Γ_1 is close to one. Flows with large aspect ratio (i.e., for large diameter) exhibit more rolls, as reported in a recent paper by Paliwal et al. (2012). It is important to note that the large-scale structures exist even in turbulent convection.
- The hot and cold plumes circulate in the azimuthal direction. This is due to the azimuthal symmetry of the system. The time period for the circulation is approximately $2\pi r/V_\phi$, where r is the average radius of the annulus, and V_ϕ is the average azimuthal velocity. The vertical velocity measured by the probes near the wall in the mid plane reverses its sign as exhibited in Fig. 7; this phenomena is known as flow reversal (Paul et al., 2010). Similar results were observed by Paul et al. (2010) in two-dimensional convective flow with periodic boundary condition along the horizontal direction. See (Movies: 2d) for an illustration of flow patterns in two-dimensional geometry.
- We observe leftward or rightward swirling of the flow. This is due to azimuthal component of the velocity. We observe similar patterns in the two-dimensional convective flow of Paul et al. (2010) under the no-slip boundary condition (Movies: 2d).
- The presence of a pair of rolls and their azimuthal movement are somewhat robust patterns, and they are observed for various choices of the boundary conditions on the lateral, top, and bottom walls.

After the above discussion on the roll structures, we describe the properties of the circumferential temperature difference (CTD) in the annulus. The study of CTD of the PFBR assembly is quite important since the higher CTD can damage the system.

3.2. Circumferential temperature difference

We measure the temperature at bottom, middle, and top of the annulus using four probes each (those labeled by A–D, I–L, and E–H respectively in Figs. 3 and 4). Note that A(B) and C(D) are placed at the diagonally opposite ends of the annulus. The temperature measured by these probes are shown in the subfigures of Fig. 8(a–c). We observe that a steady state is reached at around ~200 s. The plots exhibit variability of the temperature, with fluctuations decreasing with height. Yet, noticeably, the temperature differences of the opposite probes for the bottom and middle probes are maximum. That is, if the probe A is the hottest, then the probe

Table 4
Parameters used in simulations for (a) G2.1, (b) G2.2, (c) G2.3. The symbols are described in Table 3.

T_F (K)	803	703	603	503	403
(a)					
T_{mean}	481	462	438	411	380
ΔT	47	30	21	13	3
CTD	45	32	22	13	4
Ra	1.73×10^9	1.15×10^9	8.55×10^8	5.66×10^8	1.42×10^8
(b)					
T_{mean}	472	452	430	405	380
ΔT	63	46	30	16	3
CTD	71	50	33	19	6
Ra	2.73×10^9	1.81×10^9	1.24×10^8	7.08×10^8	1.42×10^8
(c)					
T_{mean}	443	433	412	397	374
ΔT	65	50	33	17	5
CTD	64	52	34	20	6
Ra	1.52×10^{10}	1.20×10^{10}	8.36×10^9	4.48×10^9	1.40×10^9

Table 5
Boundary and initial conditions of our simulations. The variables are temperature (T), velocity (U), pressure (P), turbulent diffusivity (α_t), turbulent dissipation rate (ϵ), turbulent kinetic energy (k), turbulent viscosity (ν_t).

Boundary	T	U	P ($\times 10^5$)	α_t ($\times 10^{-3}$)	ε ($\times 10^{-7}$)	k ($\times 10^{-4}$)	ν_t ($\times 10^{-3}$)
F	T^*	0	1.11	0.83	3.68	0.58	0.83
CL	I	0	1.11	0.83	3.68	0.58	0.83
CU	I	0	1.11	2.05	5.14	1.08	2.05
AOSW	HL	0	1.11	2.05	5.14	1.08	2.05
AISW	I	0	1.11	1.44	4.41	1.44	1.44
LSW	I	0	1.11	0.83	3.68	0.58	0.83

T^*: 803, 703, 603, 503 and 403 K; I: Insulated; HL: Heat Loss.

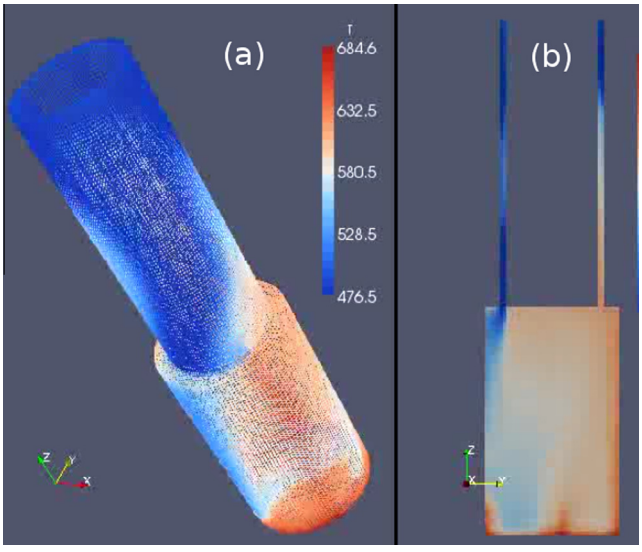

Fig. 5. For Geometry G1, a temperature profile during the steady state of the (a) full cylinder, (b) a vertical cross-section. The red and blue colors represent the rising hot and descending cold plumes respectively. (For interpretation of the references to color in this figure legend, the reader is referred to the web version of this article.)

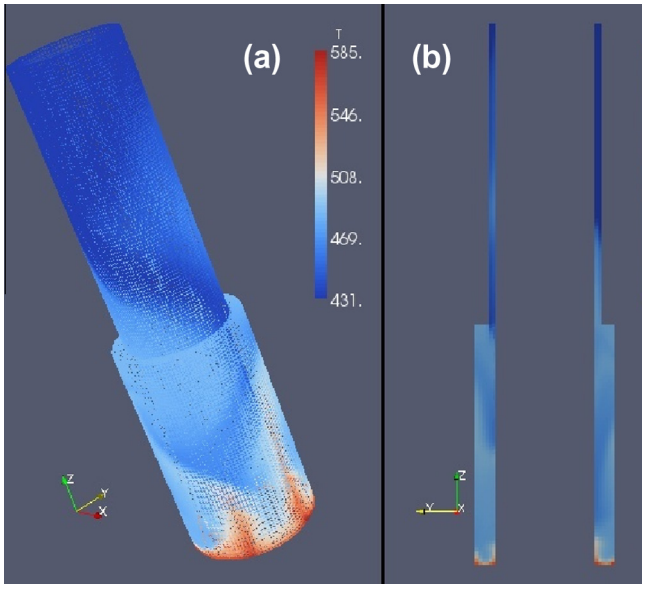

Fig. 6. For Geometry G2, a temperature profile during the steady state of the (a) full cylinder and (b) a vertical cross-section.

C would be the coldest. This feature indicates that the annulus contains a pair of convective rolls, with the hot and cold plumes positioned at the opposite ends in the annulus, consistent with our earlier results on the temperature profiles (see Figs. 5–7).

The temperature difference between the probes in PFBR is quantified using a quantity named "circumferential temperature difference (CTD)", which is computed by averaging the temperature difference measured by two opposite probes (e.g., probes A and C, or B and D). In Fig. 9(a–c) we illustrate the time series of the temperature difference during a steady state. Note that CTD is the time-averaged value of this time series.

We studied CTD for both the geometries G1 and G2 for various Rayleigh numbers. In Figs. 10 and 11 we plot the mean value of CTD as a function of ΔT and Ra. Here ΔT is the temperature difference between the bottom and top ceiling of the annulus. The above figures illustrate that the CTD is nearly proportional to ΔT. For G1, the best fit curve is CTD = $1.1\Delta T + 1.5$ (Fig. 10(a)). The corresponding curves for G2 are CTD = $0.95\Delta T + 1.3$ (blue, G2.1),

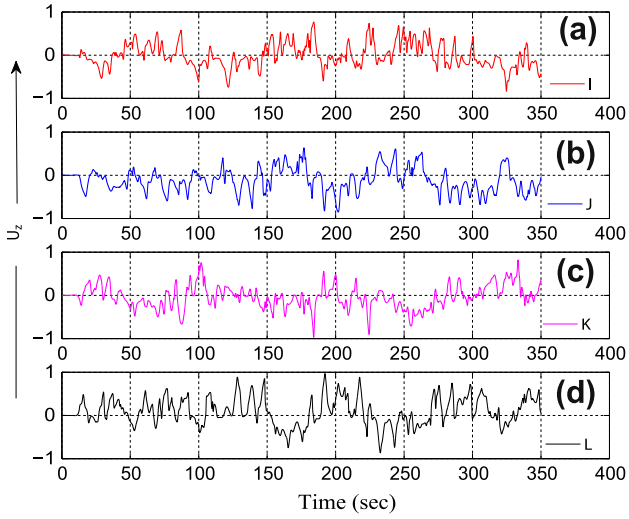

Fig. 7. Time series of the z-component of the velocity (U_z) of four probes (I, J, K, L) at the middle cross-section of the annulus. The changing sign of U_z indicates flow reversal, as reported in Paul et al. (2010).

CTD = $1.10\Delta T - 1.8$ (red, G2.2), CTD = $0.96\Delta T + 3.0$ (black, G2.3), all in Fig. 11(a). These results are consistent with that of Verma et al. (2012) where they showed that the rms value of the temperature fluctuations in turbulent convection is proportional ΔT. We also plot CTD vs. Ra for both the geometries, which also shows a linear relationship. The results CTD $\propto \Delta T$ and CTD $\propto$ Ra are consistent with each other since Ra $\propto \Delta T$. The slope of the CTD vs. Ra vary for different plots due to the L^3 factor in Ra. Note that $L = 1$ for G2.1 and G2.2 configurations, while $L = 1.8$ for G2.3. Hence, the slope of Ra vs. ΔT curve for the G2.3 configuration is around $1.8^3 \approx 5.8$ times smaller than those for G2.1 and G2.2 configurations.

The variation of CTD with the height of the annulus is shown in Fig. 12 (for G1). We have employed a fourth-order spline to fit a curve through the measured values. The figure shows that the CTD decreases from the bottom to the top, apart from minor fluctuations, which are due to the dynamic nature of the convection. The decrease of CTD with height is due to the fact that the plumes become weaker with height, consistent with the aforementioned results on the time series of the temperatures. Similar pattern emerge for the G2 configurations as well.

4. Conclusions

The Argon gas in the annulus of the PBFR exhibits turbulent convection. In this paper we describe the results of our numerical simulations of the turbulent flow performed using an open source code OpenFOAM. We employed RANS scheme and k–ϵ model in our simulations. We analyzed the flow for two sets of geometries with Rayleigh numbers ranging from 10^8 to 10^{10}. We observe several interesting features in the turbulence convection of Ar. A summary of our result are described below.

- The system exhibits a pair of convective rolls, with a hot plume rising from one end, and the cold plume descending from the opposite end, a result consistent with earlier experiments and numerical simulations (Baldassari et al., 1984; Goldstein and Joly, 1979; Hemanath et al., 2007; Meikandamurthi et al., 1991; Velusamy et al., 1998; Vijayan et al., 1986; Yamakawa and Sakai, 1986). This feature is similar to the convective patterns in a box with periodic boundary condition along the horizontal direction (Paul et al., 2010). A pair of rolls is observed for aspect ratios around one. The number of convective rolls is more for larger aspect ratios (ϵ^{-1}), as observed in recent simulations of Paliwal et al. (2012).

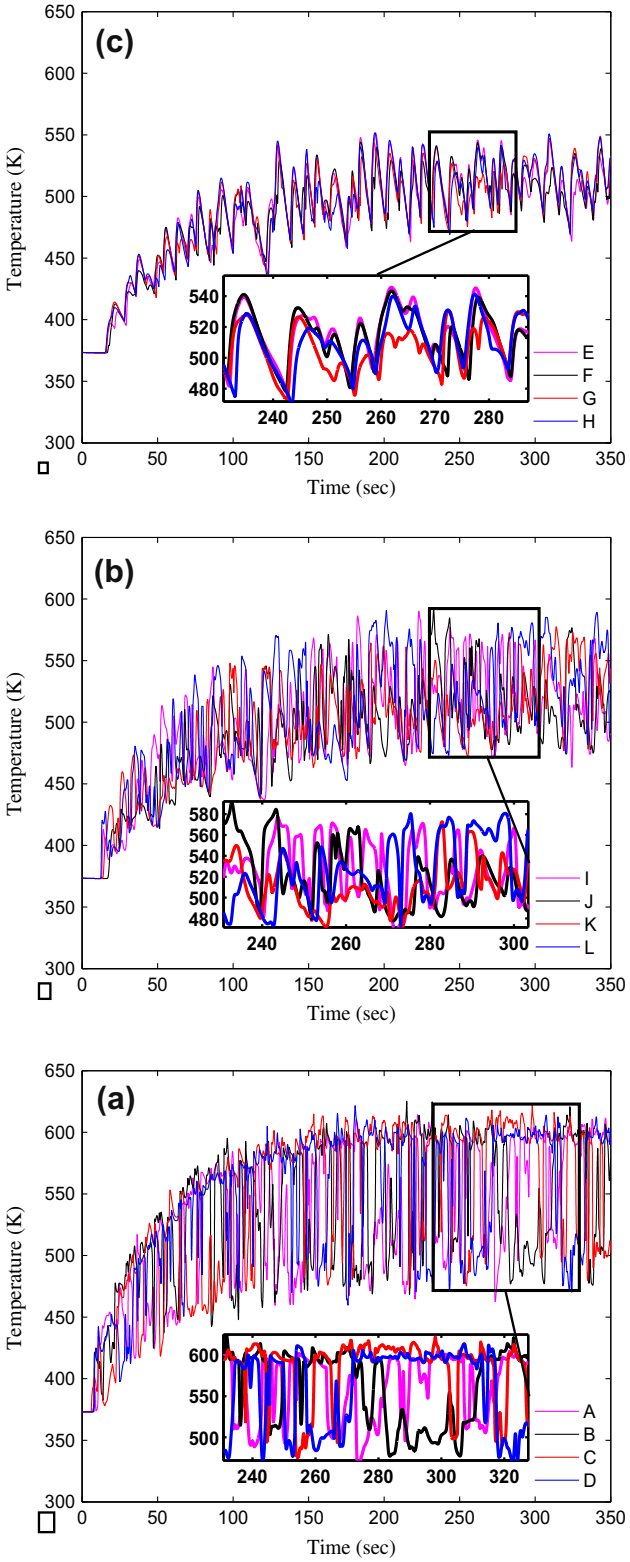

Fig. 8. Time series of the temperatures recorded by the four probes for G1 configuration with the floor temperature at 803 K: (a) at the entrance cross-section (probes A, B, C and D), (b) middle cross-section (I, J, K and L), and (c) top cross-section (E, F, G and H).

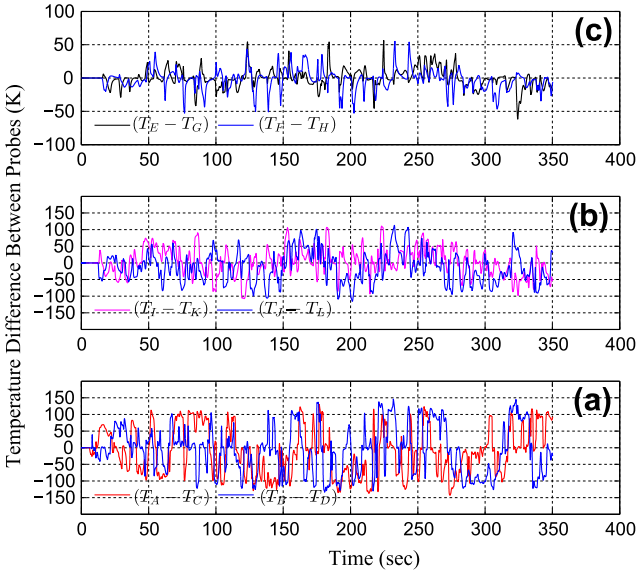

Fig. 9. Time Series of the temperature differences measured by the diametrically opposite probes at the three locations of the annulus (a) at the entrance, (b) middle, and (c) at the top.

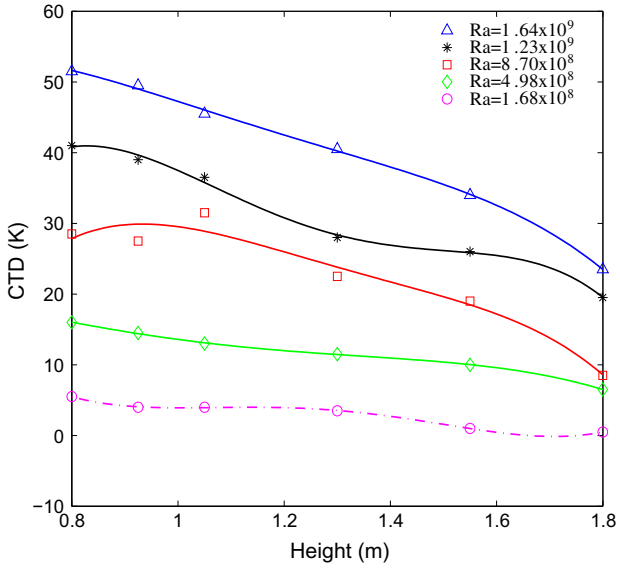

Fig. 12. For G1, plots of the circumferential temperature difference (CTD) vs. height for various Ra.

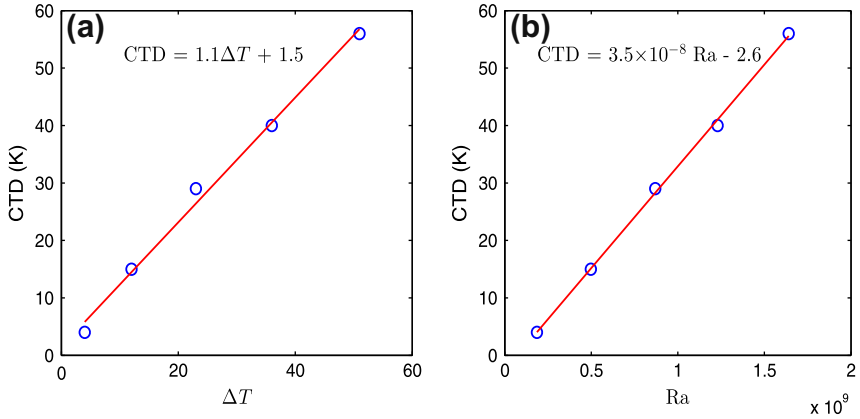

Fig. 10. (a) For G1, plot of the circumferential temperature difference (CTD) vs. ΔT, (b) CTD vs. Ra. Here CTD $\propto \Delta T$ and CTD $\propto$ Ra.

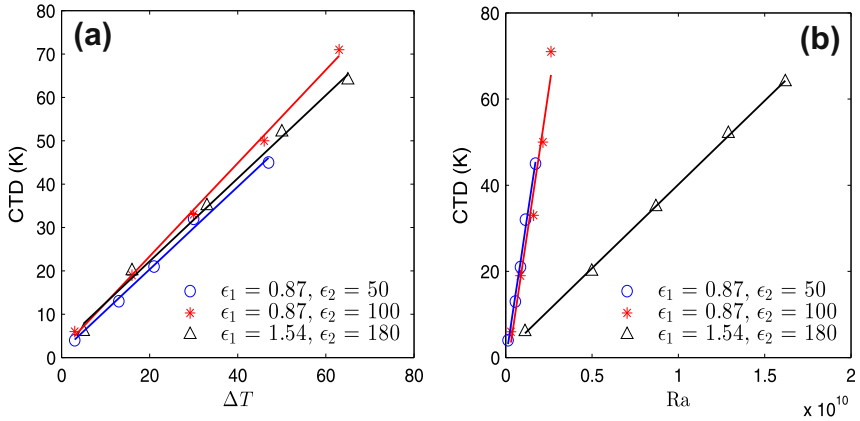

Fig. 11. (a) For G2, plots of the circumferential temperature difference (CTD) vs. ΔT, (b) CTD vs. Ra (blue G2.1, red G2.2, black G2.3). CTD $\propto \Delta T$ and CTD $\propto$ Ra. The slope of Ra vs. ΔT curve for the G2.3 configuration is around $1.8^3 \approx 5.8$ times smaller that those for G2.1 and G2.2 configurations due to the size effect. (For interpretation of the references to color in this figure legend, the reader is referred to the web version of this article.)

- The convective patterns move along the azimuthal direction, leading to dynamic variation of temperature and velocity. We observe flow reversals, similar to those reported by Paul et al. (2010).
- The design of the PFBR requires that the temperature difference within the annulus should not be too large. We studied the circumferential temperature difference (CTD) between two probes placed opposite to each other inside the annulus. We observe that the CTD is proportional to ΔT, the temperature difference between the top and bottom ceiling of the annulus, as well as CTD $\propto$ Ra. These findings are consistent with the earlier work of Verma et al. (2012) where they relate the temperature fluctuations to the temperature difference between the bottom and top plates. It however differs from the earlier results on PFBR where CTD varies logarithmically with Ra (Meikandamurthi et al., 1991; Hemanath et al., 2007). We believe that the linear fit is more suitable than the logarithmic fit, however, this observation needs additional experimental and numerical verification. This is one of the of the most important results of our paper. If applicable, it will be very valuable for the design of PFBR.
- We observe that the CTD decreases monotonically with height, consistent with earlier experimental and numerical findings (Lenoir and Goldstein, 1981; Vijayan et al., 1986). The decrease is due to weakening of the thermal plumes with height.

Our numerical results, based on RANS scheme with k–ϵ model, are in general agreement with the earlier experimental and numerical results with several new observations. In addition, they are in same lines as the direct numerical simulations of Rayleigh-Bénard convection (Paul et al., 2010; Verma et al., 2012). However, the application of k–ϵ model does casts a shadow of doubt, and we need to verify some of the results with direct numerical simulations, even though they are more expensive. We hope that the future work in this direction will provide more concrete picture of the flow patterns in the PFBR annulus.

Acknowledgments

This work was supported by a research grant from IGCAR. We are thankful to Drs. S.C. Chetal, P. Chellapandi, K. Velusamy, and K. Natesan (IGCAR, Kalpakkam, India) for helpful discussions and for providing experimental data. We are grateful to Supriyo Paul, M.S. Kalra, Vikram Rathore, and Pankaj Wahi for suggestions and help in computations.

References

Baldassari, J.P., Durin, M., Severi, Y., Pradel, P., 1984. Open azimuthal thermosyphon in annular space, comparison of experimental and numerical results. In: Proceedings of International Conference on Liquid Metal Engineering and Technology, BNES, London, UK, pp. 463–467.

Barrett, R., Berry, M., Chan, T.F., Demmel, J., Donato, J.M., Dongarra, J., Eijkhout, V., Pozo, R., Romine, C., Vorst, H.V.D., 1994. Templates for the Solution of Linear Systems: Building Blocks for Iterative Methods,. SIAM, Philadelphia.

Dwight, E., 1972. American Institute of Physics Handbook. third ed.. McGrawHill, New York.

Goldstein, S., Joly, J., 1979. Thermal analysis of penetrations of a LMFBR. In: Proceeding of Fifth International Conference on Structural Mechanics in Reactor Technology, Fifth SMiRT, Berlin, Germany.

Hemanath, M.G., Meikandamurthy, C., Ramakrishnan, M., Rajan, K.K., Rajan, M., Vaidyanathan, G., 2007. Cellular convection in vertical annuli of fast breeder reactors. Ann. Nucl. Energy 34, 679–686.

Issa, R.I., 1985. Solution of the implicitly discretized fluid flow equations by operator-splitting. J. Comput. Phys. 62, 40–65.

Lenoir, G., Goldstein, S., 1981. Thermal hydraulics of the annular spaces in roof slab penetrations at liquid sodium cooled fast breeder reactor. In: Proceedings of Sixth International Conference on Structural Mechanics in Reactor Technology, E, 1/6, Sixth SMiRT, Paris, France.

Meikandamurthi, C., Rajan, M., Kale, R.D, 1991. Experimental investigations for convection studies in top annuli. In: Proceedings of the Indo-Soviet Seminar on Thermophysics and Thermohydraulics of FBR's, Kalpakkam, India.

Movies: 2d. Movies of Convective Patterns in 2D with the Horizontal Direction as Periodic. <http://home.iitk.ac.in/~mkv/Videos/Convection.html> (Videos VC-1, VC-2).

Movies G12. Movies of convective patterns in G1 and G2. <http://home.iitk.ac.in/~mkv/Videos/Convection.html> (Videos VC-16, VC-17).

Paliwal, P., Parthasarathy, U., Velusamy, K., Sundararajan, T., Chellapandi, P., 2012. Characterization of cellular convection of argon in top shield penetrations of pool type liquid metal fast reactors. Nucl. Eng. Des. 250, 207–218.

Patankar, S.V., 1980. Numerical Heat Transfer and Fluid Flow. Taylor & Francis.

Paul, S., Kumar, K., Verma, M.K., Carati, D., De, A., Eswaran, V., 2010. Chaotic traveling rolls in two-dimensional Rayleigh–Bénard convection. Pramana 74, 75.

Timo, D.P., 1954. Free Convection in Narrow Vertical Sodium Annuli KAPL-1082 Knolls Atomic Power Laboratory, Scenectady, New York, USA.

Velusamy, K., Vaidyanathan, G., Sundararajan, T., Chetal, S.C., Bhoje, S.B., 1998. Natural convection in narrow component penetrations of PFBR roof slab. J. Energy, Heat Mass Transfer 20, 1–11.

Velusamy, K., Chellapandi, P., Chetal, S.C., Baldev, R., 2010. Overview of pool hydraulic design of Indian prototype fast breeder reactor. Sādhāna 35, 2, 97–12.

Verma, M.K., Mishra, P.K., Pande, A., Paul, S., 2012. Scaling of field correlations and heat transport in turbulent convection. Phys. Rev. E 85, 016310.

Vijayan, P.K., Saha, D., Raj, V.V., 1986. Studies on natural convection in vertical annuli heated from below. In: Proceedings of Eighth International Heat Transfer Conference, vol. 4, San Fransisco, California, USA, pp. 1563–1568.

Yamakawa, M., Sakai, T., 1986. Analysis of natural convection in narrow annular gaps of LMFBR. J. Nucl. Sci. Technol. 23, 5, 451–46.